Effects of the resonant modes on the magnetic footprint patterns in a tokamak wall

Elton C. da Silva
Instituto de Física, Universidade de São Paulo, 5315-970 São Paulo, São Paulo, Brazil

Marisa Roberto
Instituto Tecnológico de Aeronáutica, Centro Técnico Aeroespacial, Departamento de Física, 12228-900 São José dos Campos, São Paulo, Brazil

Iberê L. Caldas
Instituto de Física, Universidade de São Paulo, 5315-970 São Paulo, São Paulo, Brazil

Ricardo L. Viana
Departamento de Física, Universidade Federal do Paraná, 81531-990 Curitiba, Paraná, Brazil

(Received 24 May 2005; accepted 20 February 2006; published online 12 May 2006)

Magnetic footprints, or deposition patterns of chaotic magnetic field lines in a tokamak wall, are studied for a configuration with resonant modes due to an ergodic limiter. The formation of magnetic footprints using a nontwist symplectic mapping for a nonmonotonic safety factor radial profile is investigated numerically. The radial position of the resonant mode we focus on changes drastically the magnetic footprints. Deeper resonant modes produce a concentrated field line deposition pattern, whereas a resonant mode closer to the plasma edge yields a broader deposition pattern. Although these shearless equilibria can present robust transport barriers, the magnetic footprints are still present and can deteriorate the plasma confinement quality. © *2006 American Institute of Physics*. [DOI: 10.1063/1.2186047]

I. INTRODUCTION

In the study of plasma-wall interactions in tokamaks, a great deal of efforts have been put into the study of particle transport in the tokamak outer plasma column, and how such processes affect the tokamak wall.[1,2] If the heat and particle loadings are too spatially localized, for example, sputtering processes occurring on the wall may release contaminants into the plasma column, deteriorating the overall confinement quality.[3] Hence, various ingenious techniques have been developed in order to uniformize the spatial distribution of particle and heat transport in the tokamak outer region as the use of chaotic magnetic field lines generated by an ergodic limiter.[4–7]

However, this initial expectation has been rather frustrated by a series of experimental results obtained in many tokamaks in which ergodic limiters were mounted, which often pointed out to a nonuniform distribution of field lines hitting the tokamak wall.[8–13] The term *magnetic footprints* has been coined to indicate the deposition pattern of field lines in the tokamak wall.[14] It should be remarked that the information conveyed by the magnetic footprints does not reflect necessarily the actual pattern of particle loading, but only a lowest-order description (guiding-center motion) which can be improved by adding drift and curvature effects.

Further theoretical work, focusing on the mathematical properties of the chaotic field line region, has pointed out that the nonuniformity of the field line deposition patterns is due to the fractal nature of the underlying manifold structure (homoclinic tangles).[14–16] Accordingly, we expect in general grounds that the distribution of magnetic footprints be fractal. This finding agrees more closely with the experimental results than the original claim of a uniform distribution of chaotic field lines over the tokamak wall.

The purpose of this paper is twofold. First, we wish to investigate the effect of considering the radial position of a resonance on the deposition pattern of magnetic footprints. The chaotic magnetic field will be produced by an ergodic magnetic limiter (EML), which creates resonances in the plasma like several other external coil systems. The ergodic limiter field can be designed to excite resonances closer or farther from the tokamak wall, depending on the mode numbers chosen for the limiter winding.[17]

Second, we consider modifications of the tokamak equilibrium field, in that it can be obtained from a monotonic or nonmonotonic safety factor profile. Although monotonic profiles are far more well known, nonmonotonic profiles have been suggested to yield improved tokamak performance due to a substantial reduction of transport through barrier formation.[18–20] Whether or not the existence of such a barrier would affect the nature and/or distribution of magnetic footprints was hitherto not known.

The generation of very long chaotic magnetic field line trajectories is required for computing magnetic footprints with a graphical resolution good enough to put into evidence their fractal nature. Since direct numerical integration of field line equations is a very time-consuming task, we use an analytically obtained area-preserving field line map.[17] The equilibrium field was chosen from an approximated analytical solution of the Grad-Schlüter-Shafranov equation in a convenient coordinate system.[21,22] Varying the safety factor profile parameters we can study both monotonic and nonmonotonic configurations. Likewise, the perturbing magnetic field

from an ergodic limiter is designed in such a way that the integrability of the field line configuration is broken and Lagrangian chaos is possible. We can choose parameters so as to excite a main resonance (whose partial destruction ultimately causes the appearance of chaos) in a desired radial location.

Our analytical mapping has been used in previous works to investigate the homoclinic tangles underlying chaotic field line regions in the outer tokamak region, when monotonic safety profiles are used.[15,23] The formation of a transport barrier, in the case of nonmonotonic profiles, has been also put into evidence with the help of this map.[24] This work aims to complete, at least in part, this investigation, by considering both profiles from the point of view of magnetic footprints. Although we have used, for estimating parameters of the field line mapping, the TCABR tokamak of University of São Paulo, our results are valid for a wider range of similar machines.

In particular, the ergodic limiter in the TCABR has been designed to control plasma oscillations.[25] We remark that measurements of the vacuum magnetic field of a prototype (mounted outside the tokamak TCABR) are reported in Ref. 26. As far as other tokamaks are concerned, the ergodic limiter has been used in TORE SUPRA to improve plasma confinement.[27] Moreover, there are recent related works from the TEXTOR[28] and the D3D groups.[29]

The rest of this paper is organized as follows: in Sec. II we review the model fields for the tokamak equilibrium and the ergodic limiter perturbation, and an analytically obtained field line mapping. Section III presents our numerical results concerning invariant sets, escape patterns, and magnetic footprints, where both monotonic and nonmonotonic profiles are considered. Our conclusions are left to the last section.

II. MODELS FOR THE EQUILIBRIUM AND THE LIMITER FIELDS

The choice of a convenient coordinate system to describe magnetic field line geometry is chiefly determined by the better attainable agreement between coordinate surfaces and magnetic flux surfaces of the plasma confinement system. In this spirit, we have chosen the nonorthogonal polar-toroidal coordinates $(r_t, \theta_t, \varphi_t)$, given by[22]

$$r_t = \frac{R_0'}{\cosh\xi - \cos\omega}, \quad \theta_t = \pi - \omega, \quad \varphi_t = \Phi, \tag{1}$$

where R_0' is the magnetic axis radius and (ξ, ω, Φ) are the toroidal coordinates. The coordinate surfaces r_t=const are displaced with respect to the tokamak geometric axis so as to emulate the Shafranov shift effect.[22]

Magnetic surfaces are characterized by nested surfaces of r_t=const, for which the safety factor reads[24]

$$q(r_t) = q_c(r_t)\left[1 - 4\left(\frac{r_t}{R_0'}\right)^2\right]^{-1/2},$$

$$q_c(r_t) = q_c(a)\frac{r_t^2}{a^2}\left[1 - \left(1 + \beta'\frac{r_t^2}{a^2}\right)\left(1 - \frac{r_t^2}{a^2}\right)^{\gamma+1}\Theta\left(1 - \frac{r_t}{a}\right)\right]^{-1} \tag{2}$$

with

$$q_c(a) \equiv \frac{I_p a^2}{I_e R_0'}, \tag{3}$$

where I_p is the total plasma current, a is the plasma radius, and the parameters γ and β, with

$$\beta' \equiv \beta\frac{(\gamma+1)}{(\beta+\gamma+2)}, \tag{4}$$

describe the plasma current profile.[24,30]

In the following, we will choose $q \approx 5$ at the plasma edge $(r_t = a)$. For a monotonic profile we will consider $\gamma = 3.25$ and $\beta = 0$ resulting in $q \approx 1$ at the magnetic axis. On the other hand, to obtain a nonmonotonic safety factor profile, for which there is a region of negative magnetic shear as well as a shearless radius, we adopt $\gamma = 0.75$ and $\beta = 2.80$ so as to have $q \approx 4.80$ at the magnetic axis. We will also choose parameters so that $a/R_0' = 0.26$, which is a typical value for tokamak discharges.[31]

Since the equilibrium magnetic field is axisymmetric, we may set the ignorable coordinate φ_t as a time-like variable, t (to be used as a field line parametrization), and put the field line equations in a Hamiltonian form.[32] This enables us to define angle-action variables $(\mathcal{I}, \vartheta)$ for an equilibrium Hamiltonian given by

$$H_0(\mathcal{I}) = 2\pi\int \frac{d\mathcal{I}}{q[r_t(\mathcal{I})]}. \tag{5}$$

The explicit form of the relations between these angle-action variables and the toroidal polar coordinates can be found in Ref. 17. The equilibrium flux surfaces exhibit the Shafranov shift with respect to the geometric axis and thus are not concentric with the tokamak wall, which is at a fixed position $\mathcal{I} = 0.055$ determined by the radius of the material limiter.

Figure 1(a) shows a nonmonotonic safety factor profile for a tokamak equilibrium field for which the safety factor at the plasma edge is $q(a) = 5$. The concavity of the profile is so as to have a shearless radius near $\mathcal{I} = 0.02$. We see that there are two radii for which the safety factor is equal to 4.0, for instance. As a consequence, a perturbation resonant with this mode will create two island chains centered at these radii. By way of contrast, in Fig. 1(b) we present a monotonic safety factor profile sharing the same value of $q(a)$, and which will be used in the next sections to compare results with those obtained in the nonmonotonic case. In the monotonic case there is only one resonant surface corresponding to $q = 4.0$, and thus just one island chain.

We consider an ergodic magnetic limiter design which consists of N_r slices of a pair of resonant helical windings, with adequate mode numbers and equally positioned along

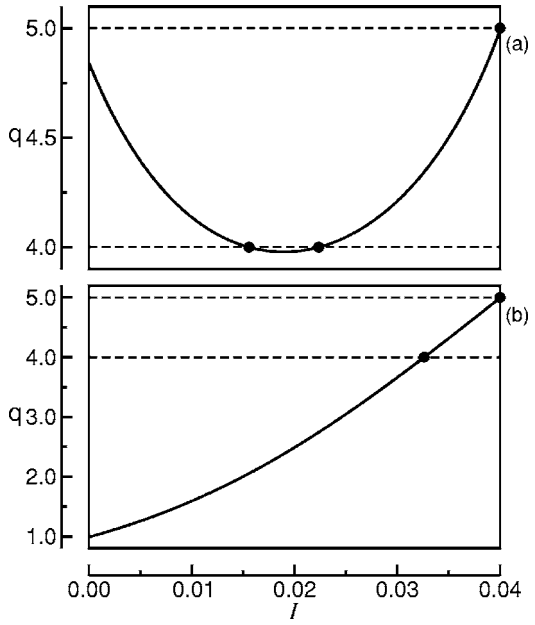

FIG. 1. (a) Nonmonotonic safety factor profile in terms of the action variable $\mathcal{I}$ and corresponding to an equilibrium field with $\gamma=0.75$, $\beta=2.80$, and $q(a)=5$. (b) Monotonic safety factor profile for $\gamma=3.25$, $\beta=0$, and $q(a)=5$.

the toroidal direction (see Fig. 2). The design of the helical windings needs to take into account the effects of the toroidal geometry, which makes the toroidal magnetic field component stronger in the inner side of the torus than in the outer one. Consequently, the magnetic field line pitch is nonuniform. We use a winding law that emulates the actual paths followed by magnetic field lines. A tunable parameter, λ, is introduced such that the variable $u_t=m_0[\theta_t+\lambda\sin(\theta_t)]-n_0\varphi_t$, where (m_0,n_0) are the poloidal and toroidal mode numbers, respectively, is constant along a field line.

A perturbing Hamiltonian, $H_1(\mathcal{I},\vartheta,t)$, describing the action of the EMLs, is obtained from the magnetic field generated by the helical windings. This magnetic field is an analytical approximated solution of the Laplace equation, supposing a vacuum field (valid for low-beta plasma only).[17] The boundary conditions are written down with the help of a singular current distribution located at the tokamak wall.

Although the equilibrium Hamiltonian $H_0(\mathcal{I})$ is integrable, the addition of a nonsymmetric perturbation, $H_1(\mathcal{I},\vartheta,t)$, caused by the EML rings, breaks the integrability

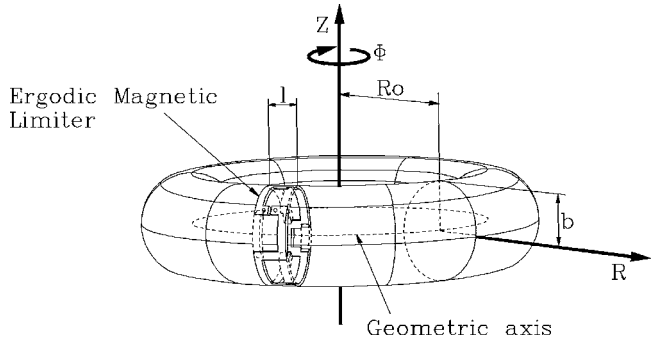

FIG. 2. Schematic diagram of one ergodic magnetic limiter (EML) ring.

of the system. Therefore, we model the action of the EML rings on the equilibrium magnetic field lines as a sequence of pulses described by the following $1+\frac{1}{2}$ degree-of-freedom Hamiltonian:

$$H(\mathcal{I},\vartheta,t)=H_0(\mathcal{I})+\epsilon H_1(\mathcal{I},\vartheta,t)\sum_{k=-\infty}^{\infty}\delta\left(t-k\frac{2\pi}{N_r}\right). \tag{6}$$

Due to the t dependence of the Hamiltonian in the form of a sequence of delta functions, it is possible to define discretized variables $(\mathcal{I}_n,\vartheta_n)$ as the corresponding values of the angle-action variables just after the nth crossing of a field line with the plane $t_k=2\pi k/N_r$ with $k=0,1,2,\ldots,N_r-1$. Proceeding in this fashion, the following area-preserving mapping can be associated with the EML Hamiltonian [Eq. (6)]:[17]

$$\mathcal{I}_{n+1}=\mathcal{I}_n+\epsilon f(\mathcal{I}_{n+1},\vartheta_n,t_n), \tag{7}$$

$$\vartheta_{n+1}=\vartheta_n+\frac{2\pi}{N_r q(\mathcal{I}_{n+1})}+\epsilon g(\mathcal{I}_{n+1},\vartheta_n,t_n), \tag{8}$$

$$t_{n+1}=t_n+\frac{2\pi}{N_r}, \tag{9}$$

where

$$f=-\frac{\partial H_1}{\partial\vartheta}, \tag{10}$$

$$g=\frac{\partial H_1}{\partial\mathcal{I}}, \tag{11}$$

$$\epsilon=2\frac{I_h l}{I_e R_0'}. \tag{12}$$

Although the map above is exactly area preserving, we stress that it has been obtained through the integration of differential equations involving delta functions, which can be ill-defined in some cases. However, there exists a rigorous method for deriving such mappings from equations with impulsive functions.[33]

Figure 3 shows two examples of Poincaré cross sections produced by the area-preserving mapping given by Eqs. (7)–(9). In Fig. 3(a), we choose $\gamma=0.75$ and $\beta=2.80$ corresponding to the nonmonotonic q profile of Fig. 1(a). The perturbing parameter $\lambda=0.4327$ is used in order to focus the perturbation on the most external surface with $q=4$. In Fig. 3(b), we choose $\gamma=3.25$ and $\beta=0$. We used $\lambda=0.5902$ in order to focus the perturbation on the $q=5$ surface. Both Figs. 3(a) and 3(b) display well-known features comprised of: (i) chains of islands which appear due to the breaking of equilibrium flux surfaces with rational q values; (ii) invariant tori formed by surviving, although deformed, flux surfaces for which q is an irrational number; and (iii) chaotic area-filling field lines which appear due to the crossing of the unstable and stable manifolds of unstable periodic orbits, as we shall discuss in more depth in the next section.

The main difference between Figs. 3(a) and 3(b) is the fact that, in the former (nonmonotonic) case, the perturbation

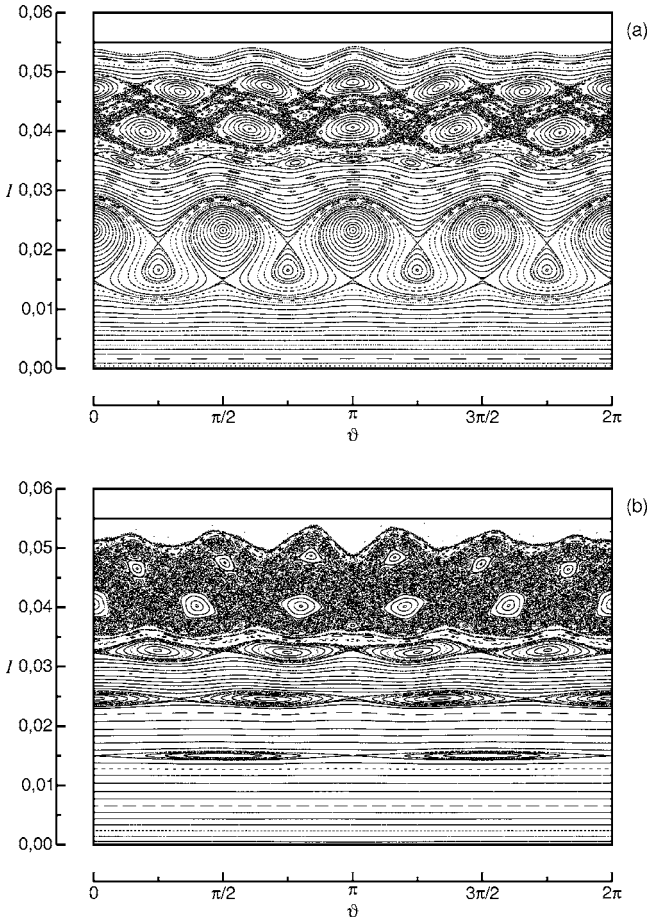

FIG. 3. Examples of Poincaré cross section produced by the EML mapping, in terms of the action-angle variables (I,ϑ). (a) Nonmonotonic q profile with $\gamma=0.75$ and $\beta=2.80$, $N_r=4$, $(m_0,n_0)=(4,1)$, $\lambda=0.4327$, and $I_h=1.4$ kA. (b) Monotonic q profile with $\gamma=3.25$ and $\beta=0$, $N_r=4$, $(m_0,n_0)=(5,1)$, $\lambda=0.5902$, and $I_h=1.4$ kA. The straight line at the top stands for the tokamak wall position.

caused by the limiter is resonant with two surfaces in the plasma bulk, since it is near the shearless radius. On the other hand, these island chains do not interact according the usual scenario of resonance overlapping, since they approach without destruction of invariant tori. The surfaces actually reconnect and the islands suffer a dimerization process, forming a single connected mesh of meandering tori, as clearly seen in Fig. 3(a). This ultimately results from the failing of many standard results, including the Kolmogorov-Arnold-Moser (KAM) theorem, for nontwist canonical mappings derived from nonmonotonic safety profiles. The chaotic orbit generated by the breakdown of integrability in this case is too small to play a significant role in the field line dynamics.

The chaotic region closer to the tokamak wall, which is also seen in Fig. 3(a), comes from a usual resonance overlapping scenario. Due to the integrability breakdown not just the resonant magnetic surfaces, but every rational surface (namely those with rational values for their safety factors) yields an island chain. The distinctive feature of resonant perturbations is that they yield larger islands than they do in nonresonant magnetic surfaces. As the safety factor near the tokamak wall is monotonic [without shear reversals, as shown by Fig. 1(a)], KAM theory holds again permitting the creation of chaotic regions at the tokamak edge.

By way of contrast, Fig. 3(b), which has been obtained by a twist mapping coming from an entirely monotonic safety factor profile [see Fig. 1(b)], presents a resonant island chain closer to the tokamak wall. We see that, for comparable limiter currents, the monotonic case was able to yield a larger chaotic region than the nonmonotonic one, where the chaotic region comes from smaller and nonresonant island chains near the tokamak wall. This has some observable effects on the escape channels of field lines hitting the tokamak wall, as shall be seen in the forthcoming section.

III. UNDERLYING STRUCTURE OF THE CHAOTIC FIELD LINES

In this section we analyze primarily the underlying structure of the chaotic region obtained for a nonmonotonic safety profile, in order to investigate the effect of using nontwist maps on the magnetic footprint patterns on the tokamak wall. The cases of resonances closer and farther from the wall are considered. Afterwards, a comparison is made with the monotonic case (twist map), for a resonance fixed at a given radial position.

A. Invariant sets

Unstable periodic orbits are in a key position in the dynamics, for they are the skeleton of a chaotic orbit. This fact was fully appreciated by Poincaré, who described in precise mathematical terms the formation of chaotic orbits many decades before they could be observed in computer screens or printouts.[34] In particular, for two-dimensional symplectic maps we focus on hyperbolic points, having both stable and unstable directions. These points can be viewed of as unstable fixed points of the map, or, if they belong to a period-p orbit, as the fixed point of the pth map iteration. From these points emanate invariant one-dimensional manifolds. Such sets are invariant in the sense that, once an initial condition is placed exactly on them, the ensuing orbit will belong to these sets. The invariant manifold is stable (unstable) provided the orbit points approach (depart) the saddle point.[35]

In conservative and integrable systems, the unstable and stable manifolds join together smoothly. However, if the system loses integrability due to a perturbation, these manifolds cross themselves an infinite number of times. The words homoclinic and heteroclinic points are used to describe an intersection between unstable and stable manifolds belonging to the same or different saddle points, respectively. Since symplectic maps are area preserving, and once the number of homoclinic or heteroclinic points are infinite (they map to one another *ad infinitum*), the manifolds are expected to undergo extremely complicated folds. The involved set of homoclinic or heteroclinic points caused by manifold intersections forms the underlying structure on which a chaotic orbit develops.[35]

Hence, the graphical representation of invariant manifolds helps to understand the nature of chaotic orbit and its consequences on the transport of field lines. This is not a trivial task, since they form a set of Lebesgue measure zero

in the phase space (i.e., given a randomly chosen point, its probability of being located exactly in the manifolds is zero), and the most we get is a numerical approximation to the true curves. There are many techniques available in the nonlinear dynamics toolbox to represent such manifolds: the iteration of linear segments along the invariant subspaces of the saddle point,[34] the sprinkler method,[36] and the saddle-straddle triple method.[37]

We have used all of these methods with practically indistinguishable results, hence we shall explain only the first method, since it is simpler than the other ones we mentioned. The above-mentioned techniques are sufficient for our purposes, but if a large number of forward or backward iterations of the mapping are necessary, numerical errors may accumulate and give a bad approximation for the invariant manifolds. In such cases, other more sophisticated techniques should be used (e.g., in Ref. 38).

We start from computing, at the saddle point chosen within the chaotic orbit, the eigenvalues and eigenvectors of the Jacobian matrix of the field line map. The unstable eigenvectors, which are related to eigenvalues whose moduli are greater than unity, span the unstable eigenspace, which turns to be simply a straight line pointing along the unstable manifold. In fact, this unstable eigenspace is tangent to the unstable manifold at the saddle point. We select a small interval aligned with the unstable subspace containing a very large number of points, and iterate forward this interval according to the mapping. It turns out that, provided we choose a number of points large enough, and the time is not so large, the resulting iterates of this interval are a numerical approximation of the unstable manifold. To obtain the stable manifold, we first set a similar interval along the stable subspace and iterate the mapping backwards. We followed the manifold for about 20 forward and backward iterations for the unstable and stable manifolds, respectively.

Our results are shown in Fig. 4 for a nonmonotonic q profile with $\gamma=0.75$ and $\beta=2.80$, and the perturbing field of an ergodic limiter with $N_r=4$ rings with mode numbers $(m_0,n_0)=(4,1)$, $\lambda=0.4327$, and a limiter current value I_h equal to 8.5% of the plasma current. For such a large limiter current there is a wide chaotic region in the outer tokamak region, as can be seen in the phase portrait [Fig. 4(a)]. Choosing a saddle in the midst of this chaotic region, we represent the stable and unstable manifolds stemming from this point in Fig. 4(b).

A typical initial condition chosen within this chaotic region will produce a trajectory which does not coincide, strictly speaking, with any of those manifolds. The trajectories, however, closely follow these directions, forward (backward) iterations of the map producing trajectories arbitrarily close to a branch of the unstable (stable) manifold. The remarkable complexity of the manifolds is the ultimate cause of the wandering behavior characteristic of chaos. The intersections of unstable and stable manifolds form a Lebesgue measure zero set of homoclinic or heteroclinic points, a numerical approximation of it being shown in Fig. 4(c). We can observe here a structure topologically equivalent to the product of two transversal Cantor-like sets. The fractal nature of Cantor-like sets will have observable consequences on the deposition patterns at the tokamak wall.

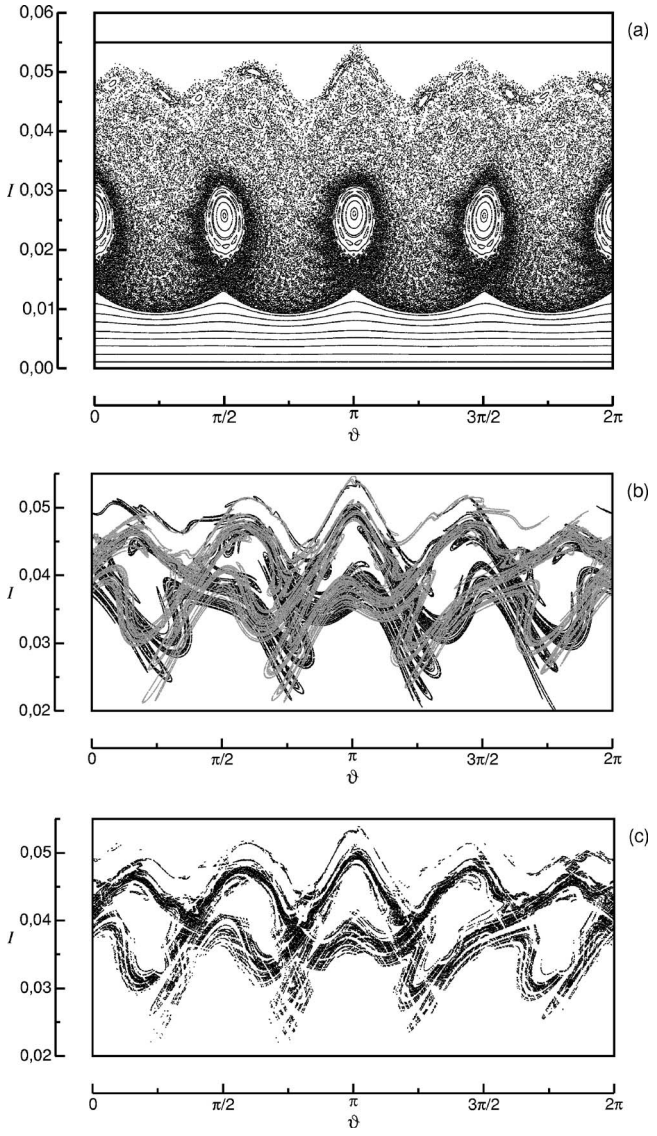

FIG. 4. (a) Poincaré cross section produced by considering a nonmonotonic q profile with $\gamma=0.75$ and $\beta=2.80$, $N_r=4$, $(m_0,n_0)=(4,1)$, $\lambda=0.4327$, and $I_h=8.5\%$ of I_p. (b) Corresponding stable (dark curve) and unstable (gray curve) manifolds. (c) Intersections among the manifolds shown in (b).

B. Magnetic footprints

In our mapping equations, the presence of a tokamak wall represents an external constraint, rather than a physical barrier, on the map orbits. Neglecting the thickness of the vessel wall, we can set the tokamak wall at the same radius as the ergodic limiter rings themselves $r_t=r_W$. Suppose that a chaotic region does intercept this constraint at one or more intervals. It is thus necessary to impose that a field line is considered lost once it reaches this radial position. The magnetic footprints are the deposition patterns of field lines from the chaotic region and which are lost due to collisions with this constraint.[14]

Starting from a typical initial condition picked up from the "bulk" of the chaotic region, the resulting field line may spend a long time n_e (measured here in number of map iterations or toroidal turns along the tokamak) before hitting the wall. The escape time n_e is measured in number of complete toroidal turns. Hence, since there are four limiters and consequently four Poincaré sections, the minimum value of n_e is 1/4.

Let us suppose that a large number $\mathcal{N}_0$ of initial conditions is chosen randomly on the chaotic region. It can be shown, by rather general arguments, that the transient times n_e for such a large number of initial conditions obey an exponential distribution. This kind of effect has been described in general terms for the average transient duration in Ref. 39 and, in the context of the present model, in Ref. 15. The actual value of n_e depends in a sensitive way on the initial condition chosen, since the unstable manifolds (or stable manifolds, if backward iterations are considered) form channels of preferential escape. Due to the extremely convoluted shape of such manifolds, it is natural to expect widely different transient times for different initial conditions.

We can distribute the $\mathcal{N}_0$ initial conditions on the tokamak wall position, uniformly choosing values of the corresponding poloidal angle ϑ, and iterating the map *backwards* in order to compute how many map iterations are necessary for the resulting orbit to come back to the wall position. This is a standardized way to compute numerically the transient time n_e. The sensitive dependence of n_e with the initial condition, provided we deal with chaotic orbits, can be appreciated in Fig. 5(a), where we depict the transient time as a function of the poloidal angle. There are regions where the dependence is quite smooth, with steps with decreasing length, but no structure. However, for an angular interval around $\vartheta=\pi$, there is a peaked region with a fine structure [see the inset of Fig. 5(a) for a magnification of this region].

This fine structure is a direct consequence of the fractal nature of the manifold skeleton which underlies chaotic dynamics there. On the other hand, the existence of a fine structure only at this interval can be understood by noting that, as Fig. 4(a) shows, the chaotic region only intercepts the tokamak wall (which is the upper margin of the figure) at a narrow interval around π. This makes for an extremely concentrated escape, which we found as being very common for nonmonotonic safety factor profiles.

The magnetic footprints themselves are depicted in Fig. 5(b), where we depict the final poloidal angle ϑ_f (when a field line has collided with the wall) as a function of the initial poloidal angle, ϑ_i, for initial conditions chosen uniformly along the poloidal curvature at the limiter radius. For many intervals the variation is smooth, with discrete steps, since the discretization of time performed to derive the mapping gives us information about what does occur after a complete turn along the torus. In the time between two intercepts with a Poincaré map we have essentially no information about the field line behavior. Even though the variation of the angle would be smooth along a complete turn, its footprint, at least as revealed by our mapping, will consist of a sequence of steps.

For the same interval centered at π as in the previous figure, a magnification of the box reveals a very involved structure. There is, however, a clear difference between the footprints characterizing smooth and fractal behavior of field lines as they hit the tokamak wall. When the behavior is smooth the footprints consist of a sequence of steps due to a finite number of perturbing rings. On the other hand, a nonsmooth behavior will produce fractal footprints, since the latter present self-similar structures, as shown by the magnification of the fractal region at the inset of Fig. 5(b). Moreover, these fractal regions correspond to field lines with large escape times and that could guide more energetic particles towards the wall.

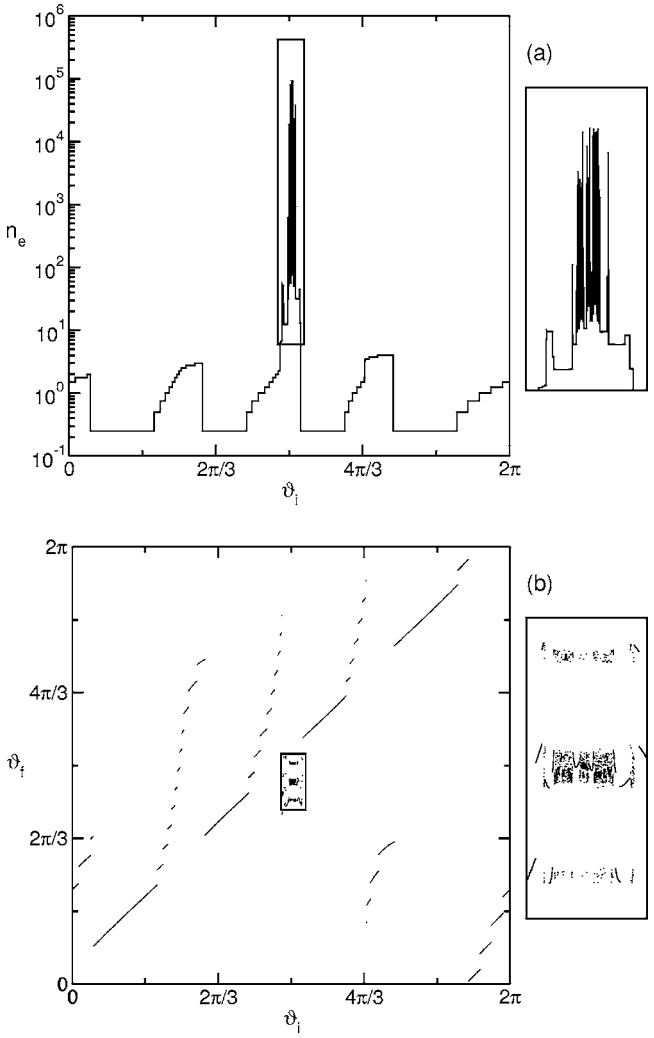

FIG. 5. (a) Number of toroidal turns a field line, which originates at the chamber wall, spends before return to the chamber wall. The inset is a magnification of the box containing a region with fine structure. (b) Deposition pattern of the longest field lines. The parameters are those of Fig. 4. A given line can escape only at the four toroidal angles where the limiters are placed.

The previous results were obtained for a limiter with mode numbers $(m_0,n_0)=(4,1)$, for which the chaotic region intercepts the tokamak wall in a very narrow interval. We can alter the limiter parameters so as to generate a chaotic region which touches the wall in more and wider intervals. Figure 6(a) demonstrates this possibility for mode numbers $(m_0,n_0)=(5,1)$. Instead of a single escape channel centered

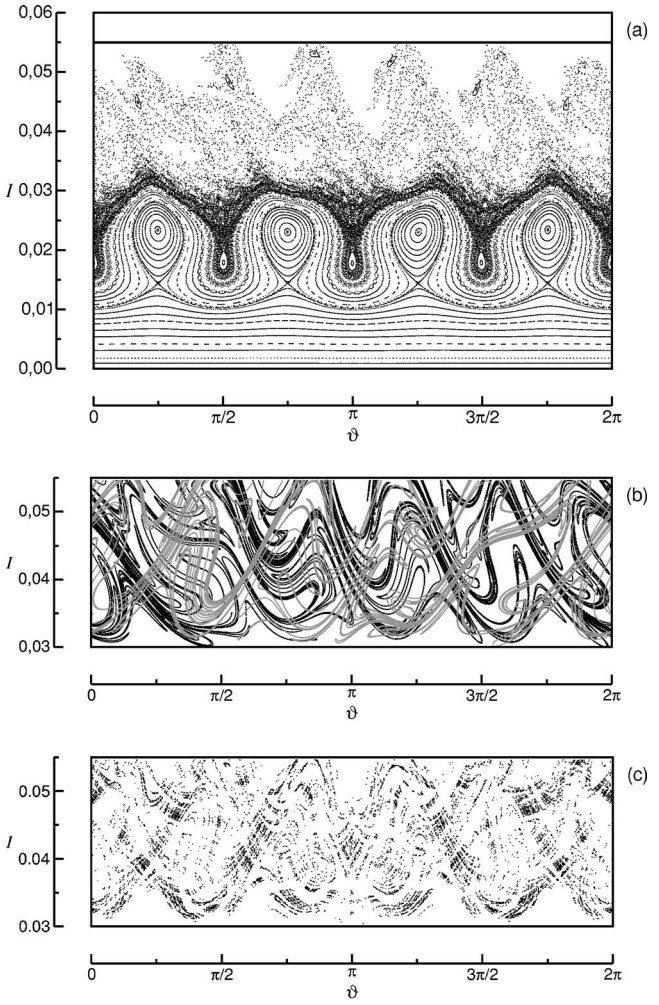

FIG. 6. (a) Poincaré cross section produced by considering a nonmonotonic q profile with $\gamma=0.75$ and $\beta=2.80$, $N_r=4$, $(m_0,n_0)=(5,1)$, $\lambda=0.5902$, and $I_h=6\%$ of I_p. (b) Corresponding stable and unstable manifolds. (c) Intersections among the manifolds shown in (b).

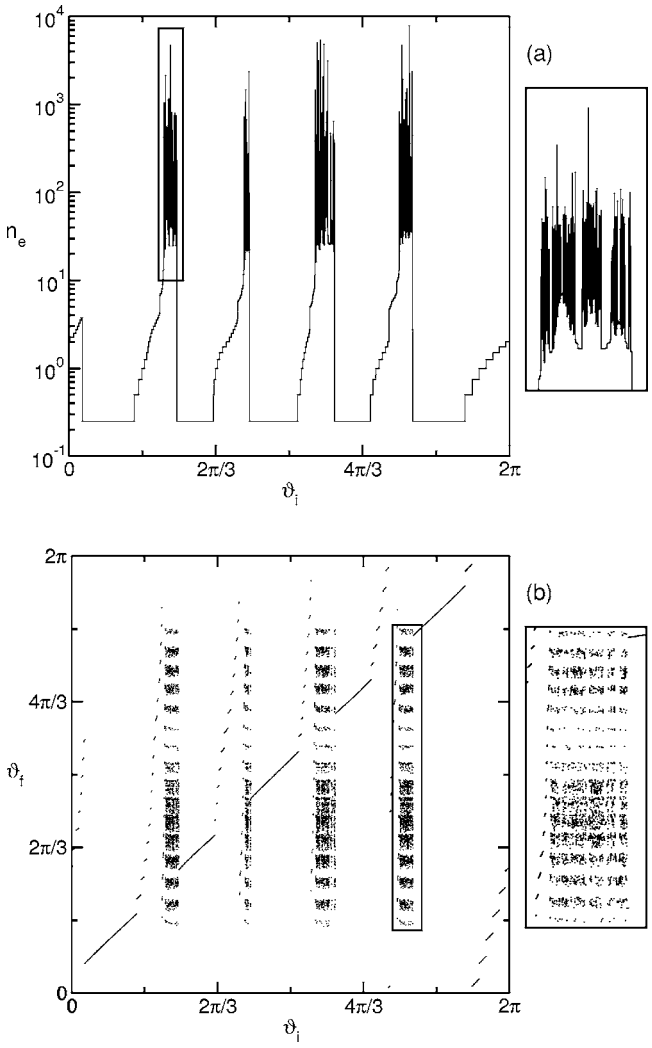

FIG. 7. (a) Number of toroidal turns a field line, which originates at the chamber wall, spends before return to the chamber wall. (b) Deposition pattern of the longest field lines. The parameters are those of Fig. 6. A given line can escape only at the four toroidal angles where the limiters are placed.

at π, we now have at least four channels. For this case, both the manifold structure [Fig. 6(b)] and heteroclinic intersections [Fig. 6(c)] are qualitatively similar to the previous case.

The consequences of having more escape channels are illustrated by Fig. 7, where both the transient times and magnetic footprints are shown for this case. At each escape channel there appears a region in which fine structure looks evident, both in the peaks of the transient time [Fig. 7(a)], or in the Cantor-like footprints of Fig. 7(b). Hence, for these mode numbers, the deposition patterns are more distributed than before. Although the field lines hit the tokamak wall through the same escape channels as before, they do so along a wider interval (of more than two-thirds of the poloidal circumference).

To understand the reason for this behavior one has to take into account that the number and the width of the intervals at which a chaotic region intercepts the tokamak wall depends on two basic factors: the mean width of the chaotic region and which resonance produces it. Although precise statements here would require a deeper mathematical treatment, the mean width of a chaotic region depends on the limiter current, as long as it is large enough to generate the region. This effect has been observed for both monotonic and nonmonotonic equilibria. On the other hand, for a same chaotic region width, the deeper the resonance producing the chaotic region is, the less it intercepts the wall for obvious reasons.

The resonance excited by mode numbers (4, 1) turned out to be deeper (i.e., farther from the wall) than the resonance induced by (5, 1). Hence, when comparing the chaotic regions for both cases, with a nearly equal limiter current, we expect the chaotic region of the latter intercepting more the wall than the former. This is not really unexpected, since the radial location of the (4, 1) resonance is slightly less than of the (5, 1) one. Even though we are dealing here with a nonmonotonic safety profile, the interval to which both resonances belong has a positive magnetic shear, i.e., there is an effectively monotonic increasing profile in that region. Moreover, this helps to explain why our results do not show a noticeable difference when monotonic profiles are considered.

Take, for instance, Fig. 8, where the chaotic regions from

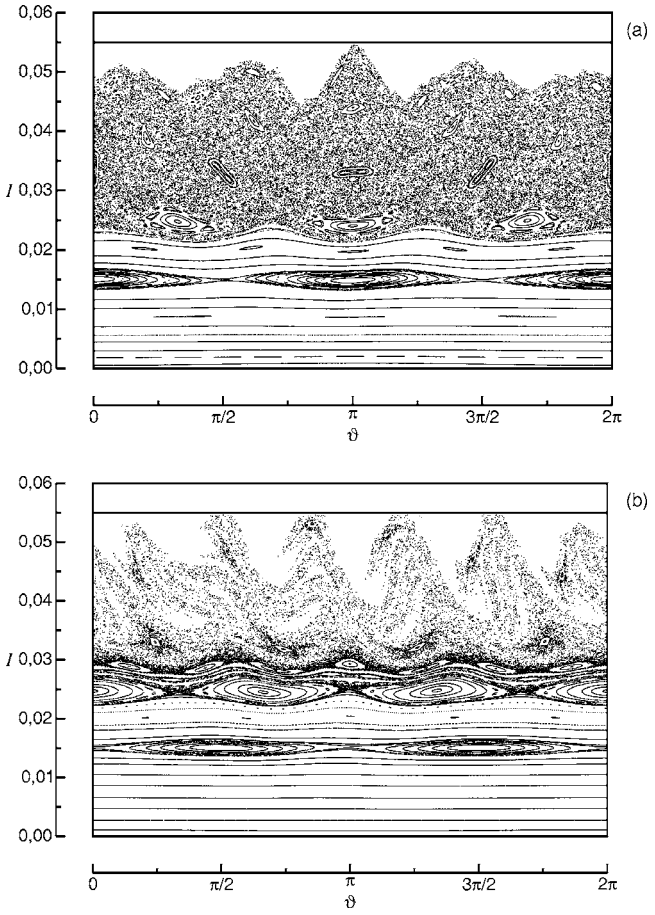

FIG. 8. Poincaré cross section produced by considering a monotonic q profile with $\gamma=3.25$ and $\beta=0$, $N_r=4$. (a) $(m_0,n_0)=(4,1)$, $\lambda=0.4327$, and $I_h=8.5\%$ of I_p. (b) $(m_0,n_0)=(5,1)$, $\lambda=0.5902$, and $I_h=6\%$ of I_p.

a monotonic profile, with $\gamma=3.25$ and $\beta=0$, are depicted in phase portraits produced by two resonances: (4, 1) and (5,1) [(a) and (b), respectively]. If we compare these portraits with their corresponding counterparts for nonmonotonic profiles [Figs. 4(a) and 6(a), respectively] we do not observe any significant difference in the number and thickness of escape channels. However, the details of the phase portraits farther from the wall are very different, since in the monotonic case there are no dimerized island chains and consequently no transport barrier.

IV. CONCLUSIONS

We summarize our findings by stating that the nonuniformity of the deposition patterns on the tokamak wall is a direct consequence of the manifold structure which underlies chaotic dynamics near the wall. The magnetic footprints thus reflect the convoluted nature of the invariant manifolds and the structures derived from the fractality of these invariant sets. The escape channels, through which the transport is enhanced, result from the intersection between the tokamak wall and the manifold structure.

The number and the distribution of these channels are determined by two factors: the mean width of the chaotic region and the resonance from which it starts. The former depends in a complicated fashion on the limiter current, whereas the second is dictated by the shape of the safety current profile in the region of interest. Since this region of interest turns to be always monotonic and increasing with the radius, regardless of the details of the safety factor profile elsewhere, our results show no noticeable difference for monotonic and nonmonotonic profiles, with respect to the chaotic region near the wall. In both cases, the deeper the resonance is from where the chaotic region starts, the more concentrated are the deposition patterns due to the existence of fewer escape channels.

The practical importance of these results lies in the fact that, although nonmonotonic profiles are expected to yield lower diffusion rates due to the generation of transport barriers, the escape pattern for field lines remains the same, as compared with the case without such barriers. Finally, if one wishes to design experiments of the sort described in this paper, and the limiter current cannot be raised above some levels, it is better to use resonances near the wall, even when nonmonotonic profiles should be used.

ACKNOWLEDGMENTS

This work was made possible through partial financial support from the following Brazilian research agencies: FAPESP (Sao Paulo) and CNPq.

[1] D. E. Post and R. Behrisch, *Physics of Plasma-Wall Interactions in Controlled Fusion* (Plenum, New York, 1986).
[2] P. C. Stangeby, *The Plasma Boundary of Magnetic Fusion Devices* (IOP, Bristol, 2000).
[3] R. Parker, G. Janeschitz, H. D. Pacher, D. Post, S. Chiocchio, G. Federici, and P. Ladd, J. Nucl. Mater. **241–243**, 1 (1997).
[4] F. Karger and F. Lackner, Phys. Lett. **61**, 385 (1977).
[5] W. Engelhardt and W. Feneberg, J. Nucl. Mater. **76/77**, 518 (1978).
[6] W. Feneberg and G. H. Wolf, Nucl. Fusion **27**, 669 (1981).
[7] T. J. Martin and J. B. Taylor, Plasma Phys. Controlled Fusion **26**, 321 (1984).
[8] S. Takamura, Y. Shen, H. Yamada *et al.*, J. Nucl. Mater. **162–164**, 643 (1989); Y. Shen, M. Miyake, S. Takamura *et al.*, *ibid.* **168**, 295 (1989).
[9] S. C. McCool, A. J. Wootton, A. Y. Aydemir *et al.*, Nucl. Fusion **29**, 547 (1989).
[10] K. H. Dippel, J. Nucl. Mater. **147**, 3 (1987).
[11] J. C. Vallet, L. Poutchy, M. S. Mohamed-Benkadda *et al.*, Phys. Rev. Lett. **67**, 2662 (1991).
[12] I. L. Caldas, R. L. Viana, M. S. T. Araujo *et al.*, Braz. J. Phys. **32**, 980 (2002).
[13] M. W. Jakubowski, S. S. Abdullaev, K. H. Finken *et al.*, Nucl. Fusion **44**, 51 (2004).
[14] S. S. Abdullaev, K. H. Finken, A. Kaleck, and K. H. Spatschek, Phys. Plasmas **5**, 196 (1998); S. S. Abdullaev, K. H. Finken, and K. H. Spatschek, *ibid.* **6**, 153 (1999); S. S. Abdullaev, Th. Eich, and K. H. Finken, *ibid.* **8**, 2739 (2001).
[15] E. C. da Silva, I. L. Caldas, R. L. Viana, and M. A. F. Sanjuán, Phys. Plasmas **9**, 4917 (2002).
[16] R. K. Roeder, B. I. Rapaport, and T. E. Evans, Phys. Plasmas **10**, 3796 (2003).
[17] E. C. da Silva, I. L. Caldas, and R. L. Viana, IEEE Trans. Plasma Sci. **29**, 617 (2001).
[18] F. M. Levinton, M. C. Zarnstoff, S. H. Batha *et al.*, Phys. Rev. Lett. **75**, 4417 (1995).
[19] E. J. Strait, L. L. Lao, M. E. Manel *et al.*, Phys. Rev. Lett. **75**, 4421 (1995).
[20] E. Mazzucato, S. H. Batha, M. Beer *et al.*, Phys. Rev. Lett. **77**, 3145 (1996).
[21] M. Y. Kucinski and I. L. Caldas, Z. Naturforsch., A: Phys. Sci. **42a**, 1124 (1987).
[22] M. Y. Kucinski, I. L. Caldas, L. H. A. Monteiro, and V. Okano, J. Plasma Phys. **44**, 303 (1990).

[23] J. S. E. Portela, I. L. Caldas, R. L. Viana, and M. A. F. Sanjuán, Int. J. Bifurcation Chaos Appl. Sci. Eng. (to be published).
[24] M. Roberto, E. C. da Silva, I. L. Caldas, and R. L. Viana, Phys. Plasmas **11**, 214 (2004).
[25] M. V. A. P. Heller, I. L. Caldas, A. A. Ferreira, E. A. O. Saettone, A. Vannucci, and I. C. Nascimento, Czech. J. Phys. **55**, 265 (2005).
[26] C. J. A. Pires, E. A. O. Saettone, M. Y. Kucinski, A. Vannucci, and R. L. Viana, Plasma Phys. Controlled Fusion **47**, 1609 (2005).
[27] T. E. Evans, M. Goniche, A. Grosman, D. Guilhem, W. Hess, and J. C. Vallet, J. Nucl. Mater. **196–198**, 421 (1992); J. A. Boedo, D. L. Rudakov, E. Hollmann *et al.*, Phys. Plasmas **12**, 072516 (2005); R. A. Moyer, T. E. Evans, T. H. Osborene *et al.*, *ibid.* **12**, 056119 (2005).
[28] M. W. Jakubowski, S. S. Abdullaev, and K. H. Finken, and the TEXTOR team, Nucl. Fusion **44**, S1 (2004).
[29] T. E. Evans, R. K. W. Roeder, J. A. Carter, and B. I. Rapoport, Contrib. Plasma Phys. **44**, 235 (2004).
[30] G. A. Oda and I. L. Caldas, Chaos, Solitons Fractals **5**, 15 (1995); G. Corso, G. A. Oda, and I. L. Caldas, *ibid.* **8**, 1891 (1997).
[31] I. L. Caldas, R. L. Viana, A. Vannucci, E. C. da Silva, M. S. T. Araujo, K. Ullmann, M. V. A. P. Heller, and M. Y. Kucinski, Braz. J. Phys. **32**, 980 (2002).
[32] P. J. Morrison, Phys. Plasmas **7**, 2279 (2000).
[33] S. S. Abdullaev, J. Phys. A **32**, 2745 (1989).
[34] E. Ott, *Chaos in Dynamical Systems*, 2nd ed. (Cambridge University Press, New York, 2002).
[35] A. J. Lichtenberg and M. A. Lieberman, *Regular and Chaotic Dynamics*, 2nd ed. (Springer-Verlag, New York, 1992).
[36] H. Kantz and P. Grassberger, Physica D **17**, 75 (1985).
[37] H. Nusse and J. A. Yorke, *Dynamics: Numerical Explorations* (Springer-Verlag, New York, 1997).
[38] D. Hobson, J. Comput. Phys. **104**, 14 (1993).
[39] C. Grebogi, E. Ott, and J. A. Yorke, Physica D **7**, 181 (1983).